



1 Brief communication: On the potential of dual-coil frequency- 2 domain electromagnetic (FDEM) systems to detect frozen 3 layers in mountain permafrost environments

4 Mirko Pavoni¹, Mauro Guglielmin², Alexander Bast^{3,4}, Stefano Ponti², Emanuele Forte⁵, Alberto Carrera¹,
5 Luca Peruzzo¹, Simone Peracchi¹, Giorgio Cassiani¹ and Jacopo Boaga¹

6 ¹ Department of Geosciences, University of Padua, Padova, Italy.

7 ² Department of Theoretical and Applied Sciences, University of Insubria, Varese, Italy.

8 ³ Climate Change, Extremes and Natural Hazards in Alpine Regions Research Center CERC, Davos Dorf, Switzerland.

9 ⁴ WSL Institute for Snow and Avalanche Research SLF, Permafrost Research Group, Davos Dorf, Switzerland.

10 ⁵ Department of Mathematics, Computer Science and Geosciences, University of Trieste, Trieste, Italy.

11 *Correspondence to:* Mirko Pavoni (mirko.pavoni@unipd.it)

12 **Abstract.** Frequency Domain Electromagnetic (FDEM) methods are still rarely applied in mountain permafrost environments,
13 such as rock glaciers. Here, we test a separable dual-coil FDEM system at four mountain permafrost sites and compare the
14 results with Electrical Resistivity Tomography (ERT), the most commonly geophysical method applied in these environments.
15 The comparison shows that FDEM can reproduce key subsurface features identified by ERT and highlights the potential of
16 separable dual-coil FDEM systems for a straightforward, preliminary, first-order assessment of subsurface structures in
17 mountain permafrost environments.

18 1 Introduction

19 Rock glaciers are widespread landforms in Alpine regions and can be used as proxies for the presence of mountain permafrost.
20 Their internal structure is typically highly complex and heterogeneous, consisting of varying proportions of ice, liquid water,
21 coarse blocks and debris, finer sediments, and air-filled void, which challenges subsurface characterization (Phillips et al.,
22 2023). Geophysical methods are commonly used to investigate the internal structure of rock glaciers in a non-invasive manner.
23 Among these, Electrical Resistivity Tomography (ERT) is the most widely employed technique due to its sensitivity to frozen
24 ground and ice-rich layers (Herring and Lewkowicz, 2022). However, ERT surveys in rock glacier environments are often
25 logistically demanding, time-consuming, and prone to issues with electrode-ground galvanic contact, particularly in coarse-
26 blocky terrains (Pavoni et al., 2022). These limitations motivate the exploration of alternative geophysical methods that are
27 better suited for rapid and preliminary subsurface mapping and characterization.

28 Frequency Domain Electromagnetic (FDEM) technique is commonly used in near-surface geophysics to easily and rapidly
29 map subsurface electrical properties (Boaga, 2017). However, its application in mountain permafrost environments remains
30 limited due to specific methodological uncertainties and challenges, first and foremost the difficulty in inducing secondary
31 eddy currents in highly resistive layers, i.e., frozen ground and dry rock (Hauck & Kneisel, 2008). Recently, FDEM has been
32 applied by Boaga et al. (2020) and Pavoni et al. (2021) to estimate the active layer thickness of rock glaciers and by Pavoni et
33 al., (2023) to investigate the internal structure of the Calderone glacieret, even if strong limitations in the quantitative
34 characterization of the electrical resistivity of the investigated frozen subsurface remain.

35 This study investigates the applicability of a separable dual-coil FDEM system at four Alpine sites characterized by different
36 permafrost-related morphologies, with the aim of assessing its potential for reconstructing subsurface structures. The FDEM
37 results are compared with ERT profiles acquired at the same locations. The findings demonstrate the effectiveness of the dual-



38 coil FDEM system as a reliable and logistically efficient approach for preliminary subsurface evaluations and for identifying
39 frozen layers within mountain permafrost environments, highlighting perspectives and limitations.

40 **2 Sites description**

41 We tested the FDEM method in different sites close to the Flüela Pass (Grisons, Switzerland) and the Stelvio Pass (Central
42 Alps, Italy). The active rock glacier at Flüela Pass has a surface of heterogeneous metamorphic blocks and debris, mainly
43 amphibolites and paragneisses, with patches of finer sediments. Measurements were carried out in the central area previously
44 investigated by Bast et al. (2024), using a 94 m ERT profile with 48 electrodes at 2 m spacing and a 50 m dual-coil FDEM
45 transect with 10 points (Fig. 1a).

46 The active rock glacier at Stelvio Pass is composed mainly of metamorphic blocks (orto- and paragneiss) and scree deposits
47 with subordinate ablation till. Past geophysical studies (e.g., Cannone et al., 2003; Etzelmüller et al., 2020) suggest the presence
48 of a massive ice core. In this study, ERT was acquired with 48 electrodes at 5 m spacing, and FDEM measurements were
49 performed at 16 regularly spaced points along a 140 m profile (Fig. 1b).

50 At Le Rese di Scorluzzo, close to the active rock glacier at Stelvio Pass, a slightly lower altitude south-facing slope hosts an
51 inactive rock glacier and, a few meters east, an inactive protalus rampart (Guglielmin and Tellini, 1992). ERT transects were
52 acquired with 48 electrodes at 3 m spacing, while FDEM measurements with 6 m point spacing practically covered the ERT
53 lines (Figs. 1c–d).

54 **3 Method: Frequency Domain Electromagnetic (FDEM)**

55 The FDEM technique, based on Maxwell's electromagnetic induction equations, allows estimation of subsurface electrical
56 resistivity without direct galvanic contact with the ground. FDEM systems consist of a transmitter coil generating a time-
57 varying magnetic field, which induces eddy currents in the subsurface; these in turn produce a secondary magnetic field
58 recorded by a receiver coil. Under the low-induction-number approximation, the quadrature component of the secondary-to-
59 primary field ratio is directly related to apparent resistivity (McNeill, 1980). Investigation depth and spatial resolution depend
60 on transmitted frequency, coil separation and orientation, and subsurface conductivity. Lower frequencies and larger spacings
61 increase sensitivity to deeper layers, while higher frequencies and shorter spacings improve near-surface resolution (Pavoni et
62 al., 2023). Horizontal coplanar (HCP) and vertical coplanar (VCP) configurations probe different depths, and highly
63 conductive conditions reduce effective penetration due to signal attenuation (Boaga, 2017). Finally, apparent resistivity
64 measurements at each location are converted into vertical resistivity profiles via inversion, iteratively adjusting the model until
65 calculated responses match observed data within an acceptable error threshold (Wagner and Uhlemann, 2022).

66 **4 Data acquisition and processing**

67 Electrical Resistivity Tomography surveys were carried out using a Syscal-Pro (Iris Instruments) resistivity meter. Data were
68 acquired using a hybrid acquisition scheme combining dipole–dipole and multi-gradient multi-skip arrays (Pavoni et al., 2025).
69 Measurements were stacked three times, and all quadrupoles were acquired in direct and reciprocal configuration for reliable
70 data quality assessment (Binley and Slater, 2022). In the blocky rock glaciers of Flüela Pass and Stelvio Pass, textile electrodes
71 (Bast et al., 2025) and steel-net electrodes (Pavoni et al., 2025), wetted with salt water, were used. In the Le Rese di Scorluzzo
72 sites, characterized by finer-grained surface sediments, traditional steel-spike electrodes were used.

73 A dataset-specific filtering procedure was applied to each ERT survey. Quadrupoles with stacking and/or reciprocal errors
74 above 5% were removed, and the same value was used as the expected data error in the inversion process. Inversion modelling
75 was performed using the open-source Python software ResIPy (Blanchy et al., 2020). All models reached a final RMS misfit



76 close to 1 in a few iterations, indicating a good fit between observed and calculated apparent resistivities. Model sensitivity
77 was used to define the lateral and vertical limits of the presented resistivity models, with low-sensitivity areas indicating
78 portions of the model mainly constrained by regularization rather than by data (Fig. S2 in Supplementary Materials).
79 FDEM measurements were collected using a separable dual-coil CMD-DUO system (GF-Instruments). The instrument
80 operates at a frequency of 925 Hz and allows data acquisition with three different coil spacings (10, 20, and 40 m). Operatively,
81 receiver and transmitter coils are connected by a thin (3 mm) cable. At each site, measurements were manually acquired using
82 the HCP configuration over the entire length of each FDEM transect (see Fig. 1), while the VCP configuration was tested at
83 only a few selected points. Measurement errors were assessed through signal stacking, and the position of each measurement
84 point was approximated as the midpoint between the two coils, corresponding to the location of the data logger equipped with
85 an integrated GPS (Fig. S1, Supplementary Materials). It should be noted that, for the profiles acquired on the active rock
86 glaciers at Flüela Pass and Stelvio Pass (Figs. 1a and 1b), the FDEM transects do not cover the full length of the corresponding
87 ERT lines. This is due to difficulties in optimally positioning the coils, particularly for the longer spacing configurations (20
88 and 40 m), because of the highly irregular topography and/or steep slopes.
89 For each site and HCP configuration (10, 20, and 40 m coil spacings), the raw FDEM apparent resistivity data were smoothed
90 using a one-dimensional Gaussian filter ($\sigma = 2$) to reduce high-frequency noise while preserving the main lateral variations.
91 The inversion modelling was performed using the open-source Python software EMagPy (McLachlan et al., 2021), employing
92 a 10-layer model of regular thickness extending to 24 m depth. The model depth was defined based on the sensitivity analysis
93 of the surveys (Fig. S3 in Supplementary Materials). While a sensitivity threshold of 70% is commonly adopted for the largest
94 coil spacing (van't Veen et al., 2022), a higher value of 80% was used in this study due to the challenging field conditions and
95 the high-resistivity subsurface, which limit the induction of secondary eddy currents. A linearized inversion with L-BFGS-B
96 regularization was employed to iteratively update the model and minimize the misfit between observed and predicted apparent
97 resistivities. The optimal regularization parameter was defined using the L-curve method, and the quality of the final model
98 was evaluated using the Root Mean Square Percentage Error (RMSPE). Although RMSPE values below 5% are generally
99 considered acceptable, in this study a threshold of 10% was adopted to account for the high-resistivity environment, the
100 measurement stacking errors of approximately 10%, and the practical difficulties in optimally positioning the coils during data
101 acquisition due to rough surface conditions and complex topography.

102 **6 Results**

103 Figure 2 shows the ERT resistivity models at the survey sites. At the active Flüela rock glacier (Fig. 2a), a shallow high-
104 resistivity layer (~60–80 k Ω -m, ~5 m depth) extends from the upper (southern) section toward the frontal zone (north), with a
105 thickness of ~10 m that gradually thins toward the front and a discontinuity at ~45 m along the profile. A comparable structure
106 is observed at the active Stelvio Pass rock glacier (Fig. 2b), with higher resistivity values and thickness (>100 k Ω -m and 15–
107 30 m, respectively). In both cases, the morphology and the presence of a high-resistivity layer suggest the occurrence of ice-
108 bearing permafrost. At the Le Rese di Scorzuzzo sites, despite morphology and vegetation suggesting the possible absence of
109 permafrost, resistivity models reveal a markedly different scenario, with high-resistivity layers characteristic of a frozen
110 subsurface. In the inactive rock glacier (Fig. 2c), in the easternmost area, the top of the high-resistivity layer lies very close to
111 the surface, making it difficult to distinguish from the overlying air-filled material, while the boundary with the underlying
112 low-resistivity unfrozen sediment is clearly identifiable. In the inactive proglacial rampart (Fig. 2d), a discontinuous high-
113 resistivity layer is detected at 5–10 m depth in the central area, likely corresponding to a frozen layer, and a superficial high-
114 resistivity zone at the northern margin corresponds to coarse, air-filled deposits observed in the field.
115 Figure 3 shows the results of the FDEM data inversions. The pseudo-2D models were obtained by interpolating (kriging
116 method) the 1D vertical resistivity profiles inverted at each measurement location (orange circles in Figs. 2 and 3). At all sites,



117 the FDEM models reproduce the same resistivity patterns observed in the ERT results, although absolute resistivity values are,
118 as expected, systematically lower. At the active Flüela Pass and Stelvio Pass rock glaciers (Figs. 3a–b), a more resistive layer
119 (~500–1000 $\Omega\cdot\text{m}$) is clearly identified between two less resistive layers (~100–300 $\Omega\cdot\text{m}$) and, as in the ERT models,
120 progressively thins and disappears toward the frontal zone. At Flüela Pass, the same discontinuity detected in the ERT model
121 is evident at ~45 m along the profile. Similarly, at the Le Rese di Scorluzzo sites (Figs. 3c–d), the FDEM-derived resistivity
122 structures closely mirror those obtained from ERT, indicating the presence of high-resistivity layers and suggesting a
123 discontinuous frozen layer at both sites.

124 In all resistivity models (Figs. 2 and 3), the boundaries of the frozen layer were interpreted from resistivity values and gradients,
125 placing limits where the variation (increase at the top, decrease at the base) is steepest (Herring and Lewkowicz, 2022).

126 **7 Discussion and conclusions**

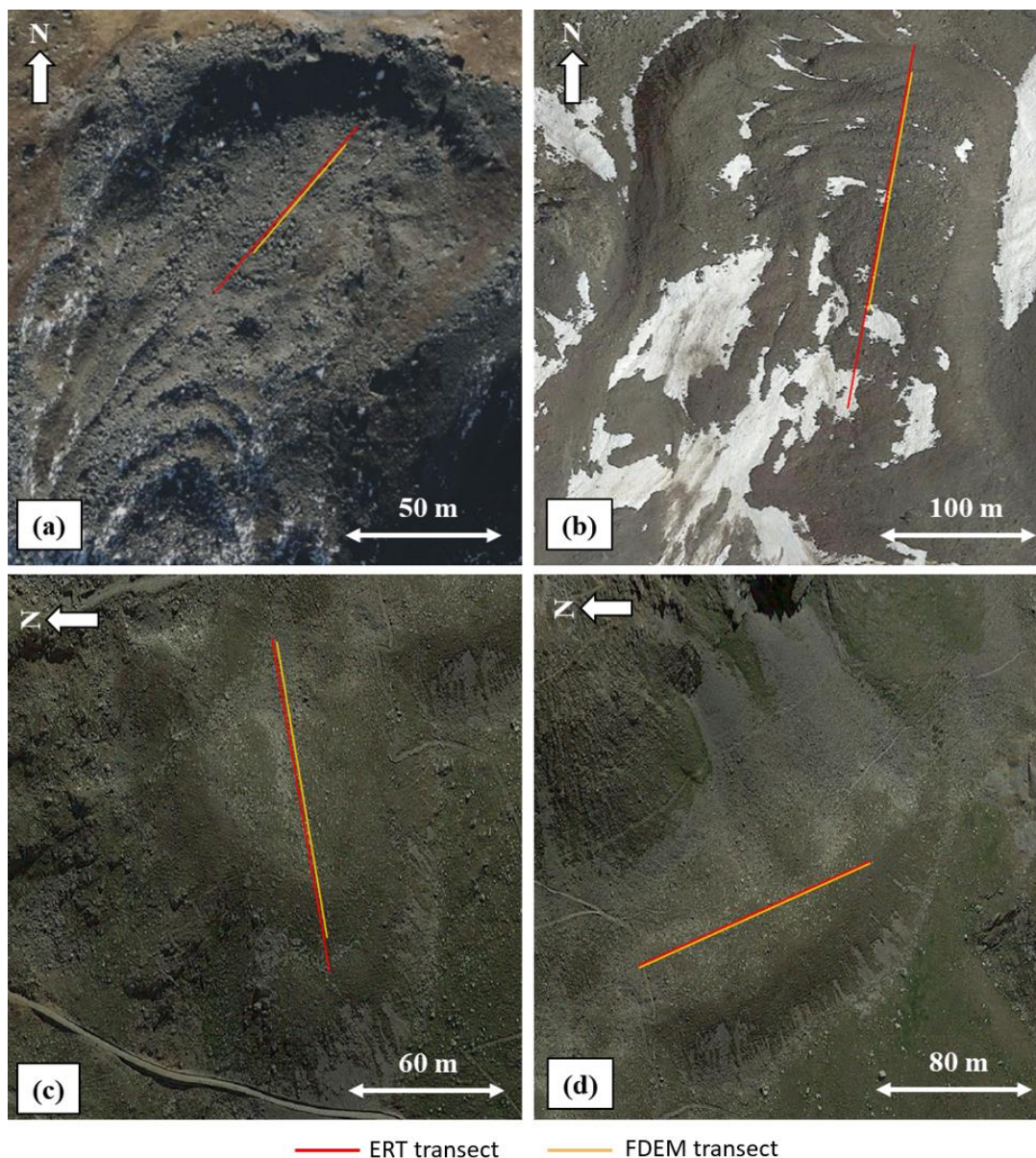
127 The results demonstrate that a separable dual-coil FDEM system with at a signal frequency of ~1 kHz, with coil spacings
128 between 10 and 40 m and HCP orientation, can reconstruct a reliable subsurface structure in mountain permafrost
129 environments. The FDEM-derived resistivity models consistently reproduce the main patterns observed in the ERT results,
130 despite systematically lower absolute resistivity values. This discrepancy is attended, given the tendency of electromagnetic
131 fields to propagate preferentially within more conductive media (Boaga, 2017), the 10 k $\Omega\cdot\text{m}$ instrumental sensitivity limit of
132 the FDEM device (Gf-instrument datasheet), the limited ability to resolve fine spatial heterogeneities (Carrera et al., 2024),
133 and the results of synthetic modelling studies. In this context, Pavoni et al. (2023) demonstrated that the separable dual-coil
134 FDEM system has a limited capability to accurately reproduce absolute resistivity values in high-resistivity frozen-layer
135 settings, although it is still able to capture the overall subsurface structure.

136 The measurements performed using the VCP configuration yielded poor results, characterized by anomalous responses,
137 including very high stacking errors, apparent resistivities up to one order of magnitude lower than those obtained with the HCP
138 configuration, and strongly negative in-phase values. These effects are likely related to signal quality, as the orientation of the
139 primary magnetic field in the VCP configuration is less favourable for subsurface penetration compared to the HCP
140 configuration, where the primary field is more efficiently coupled with the ground, facilitating the induction of eddy currents.
141 Similar limitations of VCP-oriented FDEM measurements in rock glacier environments were previously reported by Pavoni
142 et al. (2021) during active-layer investigations. Necessarily, the exclusion of the VCP configuration reduces the number of
143 apparent resistivity measurements at each measured station, resulting in a loss of vertical resolution. However, given the
144 consistently poor data quality obtained with VCP measurements and the cost of doubling survey time, the effort of acquiring
145 this configuration does not appear justified. Instead, survey efficiency can be improved by focusing exclusively on the HCP
146 configuration and increasing the number of measurement locations, thereby enhancing lateral resolution.

147 Although continuous FDEM acquisition could accelerate data collection further and yield very dense datasets, this approach
148 is difficult to implement in rock glacier environments due to the irregular surfaces and complex topography that prevent stable
149 antenna positioning during measurements. Consequently, static dual-coil FDEM acquisition in HCP configuration, with
150 antennas placed directly on the ground as illustrated in Fig. S1, represents the most practical and robust strategy.

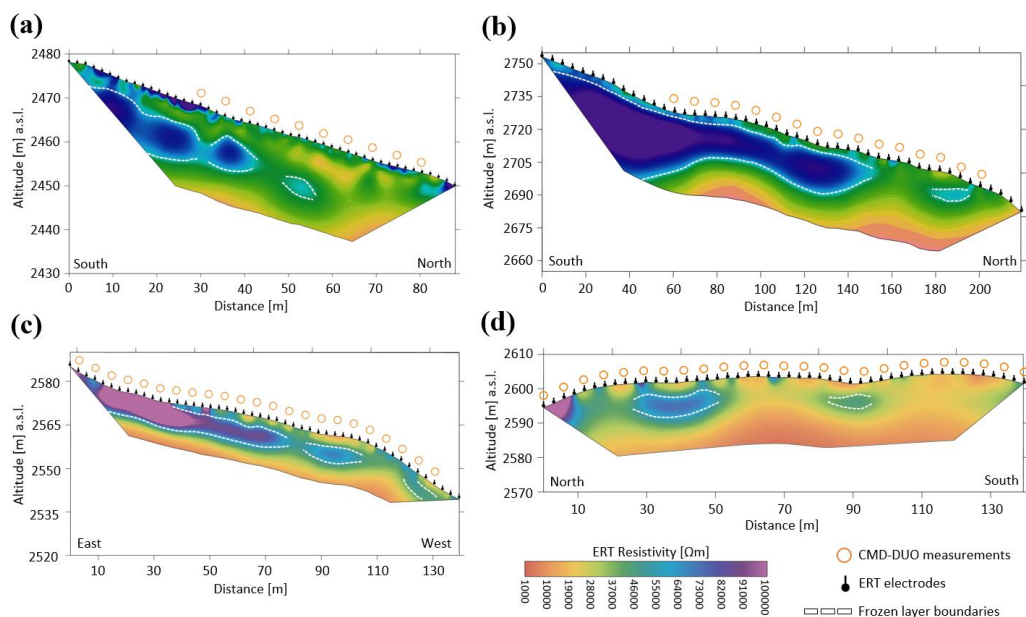
151 From a logistical perspective, the relatively low weight of the separable dual-coil FDEM system components (~5 kg per
152 antenna, ~1 kg for the data logger, and ~5 kg for connecting cables) allows deployment by small teams (2–3 operators) without
153 the relevant physical and logistical effort required for ERT surveys.

154 Overall, considering the limited logistical effort required for transport and data acquisition, the relatively straightforward data
155 processing and interpretation, the proposed separable dual-coil FDEM system represents a highly promising tool for
156 preliminary investigations, including remote areas, and for large-scale mapping of mountain permafrost distribution.



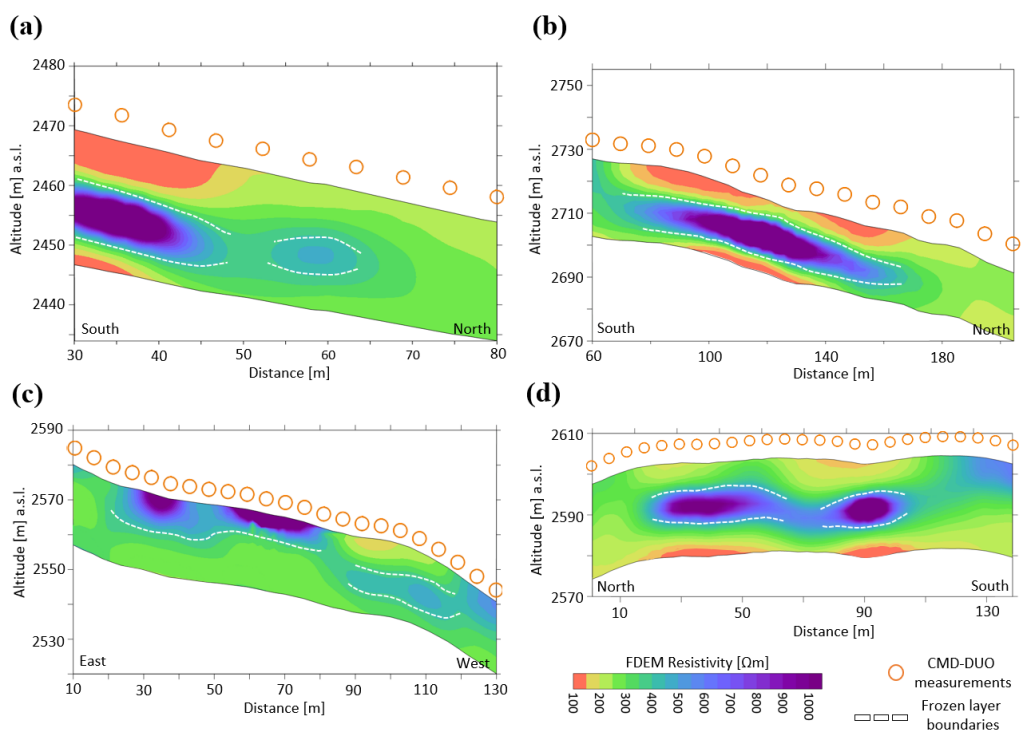
157

158 Figure 1. Satellite images of the study sites (Background imagery from Google Satellite; accessed via QuickMapServices in QGIS;
159 Imagery © Google; map data © Google) showing the ERT (red lines) and FDEM (orange lines) survey profiles. (a) Active rock
160 glacier at Flüela Pass (Switzerland; 46.746° N, 9.951° E). (b) Active rock glacier at Stelvio Pass (Italy; 46.527° N, 10.441° E). (c) Le
161 Rese di Scorluzzo inactive rock glacier at Stelvio Pass (Italy; 46.531° N, 10.420° E). (d) Le Rese di Scorluzzo inactive protalus rampart
162 at Stelvio Pass (Italy; 46.530° N, 10.421° E).



163

164 **Figure 2.** Inverted resistivity models obtained from ERT measurements at (a) the active rock glacier at Flüela Pass, (b) the active
 165 rock glacier at Stelvio Pass, (c) Le Rese di Scorluzzo inactive rock glacier, and (d) the Le Rese di Scorluzzo inactive protalus rampart
 166 at Stelvio Pass. The positions of the ERT electrodes (black point marker with stem) along the transects and the measurement points
 167 acquired with the CMD-DUO FDEM system (orange circle) are shown. The white dashed line indicates the interpreted boundary of of
 168 the inferred frozen layer.



169

170 **Figure 3.** Pseudo-2D inverted resistivity models obtained from FDEM data acquired with the CMD-DUO in HCP configuration at
 171 the sites of (a) active rock glacier at Flüela Pass, (b) active rock glacier at Stelvio Pass, (c) Le Rese di Scorluzzo inactive rock glacier,
 172 and (d) the Le Rese di Scorluzzo inactive protalus rampart at Stelvio Pass. The positions of the measurement points are marked
 173 with orange circles, and the white dashed line indicates the inferred boundary of the frozen layer.



- 174 *Data Availability Statement.* The datasets will be available upon request from the authors
- 175 *Author contributing.* MP, MG, EF, JB developed the concept of the study; MP, AB, MG, SPo, JB were involved in the data
176 acquisition; MP performed the data processing; all authors contributed to the writing and editing of the manuscript.
- 177 *Competing interests:* The contact author has declared that none of the authors has any competing interests.
- 178 *Financial support:* This study was carried out within the project of the excellence program: “The Geosciences for Sustainable
179 Development” project (Budget Ministero dell’Università e della Ricerca–Dipartimenti di Eccellenza 2023–2027
180 C93C23002690001)”.

181 **References**

- 182 Bast, A., Pavoni, M., Lichtenegger, M., Buckel, J., and Boaga, J.: The Use of Textile Electrodes for Electrical Resistivity
183 Tomography in Periglacial, Coarse Blocky Terrain: A Comparison With Conventional Steel Electrodes. *Permafrost and*
184 *Periglacial Processes*, <https://doi.org/10.1002/ppp.2257>, 2024.
- 185 Binley, A., and Slater, L.: *Resistivity and induced polarization: Theory and applications to the near-surface earth*. Cambridge
186 University Press, DOI: 10.1017/9781108685955, 2020.
- 187 Blanchy, G., Saneiyani, S., Boyd, J., McLachlan, P., and Binley, A.: ResIPy, an intuitive open source software for complex
188 geoelectrical inversion/modeling. *Computers & Geosciences*, 137, 104423, <https://doi.org/10.1016/j.cageo.2020.104423>,
189 2020.
- 190 Boaga, J.: The use of FDEM in hydrogeophysics: A review. *Journal of Applied Geophysics*, 139, 36-46.
191 <https://doi.org/10.1016/j.jappgeo.2017.02.011>, 2017.
- 192 Boaga, J., Phillips, M., Noetzi, J., Haberkorn, A., Kenner, R., & Bast, A.: A comparison of frequency domain electro-
193 magnetometry, electrical resistivity tomography and borehole temperatures to assess the presence of ice in a rock glacier.
194 *Frontiers in Earth Science*, 8, 586430., 2020.
- 195 Cannone, N., Guglielmin, M., Hauck, C., Vonder Muhll, D.: The impact of recent glacier fluctuation and human activities on
196 the permafrost distribution: a case study from Stelvio Pass (Italian Central-Eastern Alps). In: Phillips M., Springman S.M.,
197 Arenson L.U. (Eds.) *Proceedings of the 8th International Conference on Permafrost*, Zurich, Switzerland, 21 – 25 July 2003,
198 Balkema Publishers, Lisse, 1, 137 – 143, 2023.
- 199 Carrera, A., Peruzzo, L., Longo, M., Cassiani, G., and Morari, F.: Uncovering soil compaction: performance of electrical and
200 electromagnetic geophysical methods, *SOIL*, 10, 843–857, <https://doi.org/10.5194/soil-10-843-2024>, 2024.
- 201 Etzelmuller, B, Guglielmin, M, Hauck, C., Hilbich, C., Hoelzle, M., Isaksen, K., Noetzi, J., Oliva, M., Ramos, M.: Twenty
202 years of European mountain permafrost dynamics-the PACE legacy. *Environmental Research Letters*, 15 (10), 104070, 2020.
- 203 Guglielmin, M., Tellini, C.: Contributo alla conoscenza dei rock glaciers delle Alpi italiane. I rock glaciers del Livignasco
204 (Alta Valtellina). *Rivista Geografica Italiana*, 99, 395-414, 1992.
- 205 Hauck, C., Kneisel, C.: *Applied geophysics in periglacial environments*. Cambridge University Press., ISBN 9780521889667,
206 2008.
- 207 Herring, T. and Lewkowicz, A. G.: A systematic evaluation of electrical resistivity tomography for permafrost interface
208 detection using forward modeling, *Permafrost Periglac.*, 33, 134–146, <https://doi.org/10.1002/ppp.2141>, 2022.
- 209 McLachlan, P., Blanchy, G., & Binley, A.: EMagPy: Open-source standalone software for processing, forward modeling and
210 inversion of electromagnetic induction data. *Computers & Geosciences*, 146, 104561.
211 <https://doi.org/10.1016/j.cageo.2020.104561>, 2021.
- 212 McNeill, J. D.: *Electromagnetic terrain conductivity measurement at low induction numbers*, Geonics Ltd., Technical Note
213 TN-6, Mississauga, Ontario, 1980.
- 214 Pavoni, M., Sirch, F., & Boaga, J.: Electrical and electromagnetic geophysical prospecting for the monitoring of rock glaciers
215 in the Dolomites, Northeast Italy. *Sensors*, 21(4), 1294. <https://doi.org/10.3390/s21041294>, 2021.



- 216 Pavoni, M., Carrera, A., and Boaga, J.: Improving the galvanic contact resistance for geoelectrical measurements in debris
217 areas: A case study. *Near Surface Geophysics*, 20(2), 178-191, <https://doi.org/10.1002/nsg.12192>, 2022.
- 218 Pavoni, M., Boaga, J., Carrera, A., Urbini, S., de Blasi, F., & Gabrieli, J.: Combining Ground Penetrating Radar and Frequency
219 Domain Electromagnetic Surveys to Characterize the Structure of the Calderone Glacieret (Gran Sasso d'Italia, Italy). *Remote
220 Sensing*, 15(10), 2615. <https://doi.org/10.3390/rs15102615>, 2023
- 221 Pavoni, M., Peruzzo, L., Boaga, J., Carrera, A., Barone, I., and Bast, A.: Brief communication: Use of lightweight and low-
222 cost steel net electrodes for electrical resistivity tomography (ERT) surveys performed on coarse-blocky surface environments,
223 *The Cryosphere*, 19, 4141–4148, <https://doi.org/10.5194/tc-19-4141-2025>, 2025.
- 224 Phillips, M., Buchli, C., Weber, S., Boaga, J., Pavoni, M., and Bast, A.: Brief communication: Combining borehole
225 temperature, borehole piezometer and cross-borehole electrical resistivity tomography measurements to investigate seasonal
226 changes in ice-rich mountain permafrost, *The Cryosphere*, 17, 753–760, <https://doi.org/10.5194/tc-17-753-2023>, 2023.
- 227 Uhlemann, S., Peruzzo, L., Chou, C., Williams, K. H., Wielandt, S., Wang, C., ... and Dafflon, B.: Variations in bedrock and
228 vegetation cover modulate subsurface water flow dynamics of a mountainous hillslope. *Water Resources Research*, 60(2),
229 e2023WR036137, <https://doi.org/10.1029/2023WR036137>, 2024.
- 230 van't Veen, K. M., Ferré, T. P. A., Iversen, B. V., and Børgesen, C. D.: Using machine learning to predict optimal
231 electromagnetic induction instrument configurations for characterizing the shallow subsurface, *Hydrol. Earth Syst. Sci.*, 26,
232 55–70, <https://doi.org/10.5194/hess-26-55-2022>, 2022.